Progress In Electromagnetics Research, PIER 59, 299–324, 2006

MULTI-LAYER CRYSTALS OF METALLIC WIRES: ANALYSIS OF THE TRANSMISSION COEFFICIENT FOR OUTSIDE AND INSIDE EXCITATION

H. Boutayeb [†], K. Mahdjoubi, and A.-C. Tarot

IETR, UMR 6164 CNRS, University of Rennes
Ave. Général Leclerc 35042 Rennes Cedex, France

Abstract—This paper proposes a new analysis of the transmission coefficient at normal incidence for 2-D periodic crystals (also called Electromagnetic Band Gap (EBG) structures), which are finite in the direction of wave-propagation and are composed of metallic wires. The crystal is considered as a set of parallel Partially Reflecting Surfaces (PRSs), whose transmission and reflection characteristics are obtained rigorously using the Finite Difference Time Domain (FDTD) method. The transmission coefficient of the EBG structure is then obtained by using a plane-wave cascading approach considering single mode interactions between PRSs. The accuracy of the results given by the hybrid method is assessed compared to those obtained directly by the Finite Difference Time Domain (FDTD) method. The minima and maxima envelops and the resonance frequencies of the transmission coefficient are studied, with analytical expressions, for both, excitation from outside and excitation from inside. A discussion is also presented concerning the strength of the coefficient greater than one obtained when the plane-wave source is inside the EBG structure. In addition, by using a transmission line model, a normalized version for this coefficient is proposed, which considers the available power by the source.

1. INTRODUCTION

Electromagnetic bandgap (EBG) materials, also known as photonic crystals [1, 2], have been the subject of intensive research in the past few years. An important feature of these structures is their

[†] Also with INRS-EMT, University of Quebec, 800, Rue de la Gauchetière, H5A 1K6, Montréal, Canada

ability to open a bandgap that is a frequency range for which the propagation of electromagnetic waves is forbidden whatever the direction of propagation and the polarization. EBG materials are periodic structures composed of dielectric and/or metallic elements. Potential applications have been suggested in microwave and antenna domains, such as suppressing surface waves [3], creating controllable beams [4, 5], and designing high-gain antennas with a single feed [6–10].

To analyze crystals with a rectangular lattice, various methods have been proposed for calculating the scattering of the periodic structures, *e.g.*, the rigorous scattering matrix method [11], and the generalized scattering matrix method with a cascading approach [12], where the periodic structure is made from the cascading of multiple layers of PRSs, also called Frequency Selective Surfaces (FSSs) [13]. These methods are rigorous but they are typically time-consuming. In this paper, a simple modeling method based on a spectral plane-wave generalized-ray analysis with a cascading process is presented to predict the characteristics of a rectangular crystal. The proposed method does not consider the higher Floquet modes interactions between PRSs, but it reduces considerably the computational time compared to the preceding methods and it is well suited for the design process of the structure.

To our knowledge, the shapes and the resonance behaviors of the transmission coefficient for rectangular periodic crystals, which are finite in the direction of propagation, have not been studied enough. Indeed, it is of a lot of interest to be able to predict the stop-bands level and the locations of the transmission peaks in order to simplify the design process. For double layer structures, the Fabry Perot approach has been used in references [14, 15]. In this paper, new analytical results and a new parametrical study of multi-layers structures are proposed, in order to simplify the design of such structures.

Furthermore, to analyze EBG-antennas, many authors have used the characterization of the EBG structure when it is excited by a plane-wave from outside, and with an observation point outside the structure also [6, 7]. However the exciting source in the proposed antennas was inside the EBG structure. Because of the principle of reciprocity, the analysis of the transmission coefficient for a source located inside an EBG structure is equivalent to the calculation of the total wave inside an EBG structure excited from outside. This second analysis has been presented in [16], by using a ray method and in [17], where a numerical method has been proposed. However, the minima and maxima envelop and the resonance frequencies of the transmission coefficient have not been studied enough. In addition, the reason of the strength of the transmission coefficient greater than one,

obtained for inside-excitation, has not been sufficiently developed and the physical insight of this anomaly has not been sufficiently explained. In this paper, a new analysis of the frequency response of a crystal with a rectangular lattice, excited from its interior, is presented, and a discussion is also proposed concerning the strength of the coefficient greater than one obtained when the plane-wave source is inside the EBG structure. In addition, a normalized version for this coefficient is proposed, by using a transmission line model and considering the available power by the source.

2. CHARACTERIZATION OF A SINGLE PARTIALLY REFLECTING SURFACE

The Partially Reflecting Surface (PRS) of infinite and perfectly conducting metallic wires, illuminated by a plane wave at normal incidence as illustrated in Fig. 1, is considered. In this figure, P_t is the transversal period and a is the wire diameter. The coefficients t and $r = |r|e^{j\varphi_r}$ are the complex transmission and the reflection coefficients of the surface, which are computed rigourously with the Finite Difference Time Domain (FDTD) method. In the FDTD code, Floquet boundaries conditions and a thin mesh ($\triangle = Period/80$) are used. For the considered PRS, the magnitude of the transmission and reflection coefficients are plotted in Figs. 2 and 3, versus normalized frequency P_t/λ, for different values of the ratio a/P_t. The phase of the

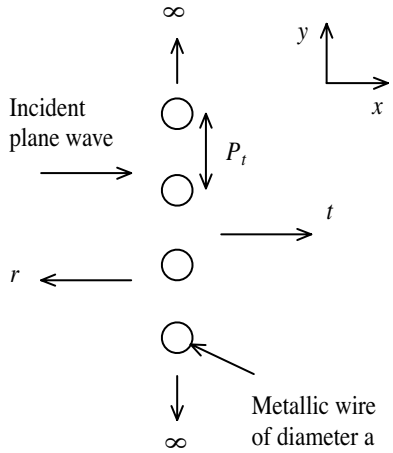

Figure 1. Partially Reflecting Surface of metallic wires.

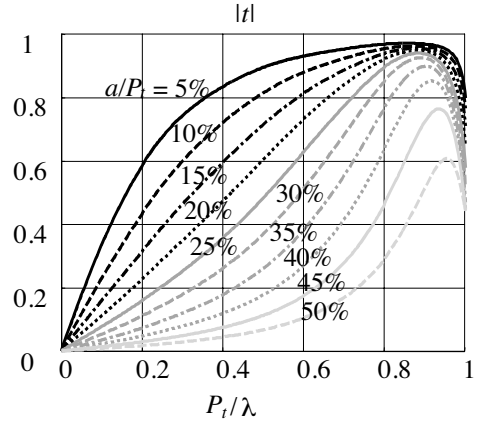

Figure 2. Coefficient $|t|$ versus normalized frequency P_t/λ for different values of a/P_t (FDTD).

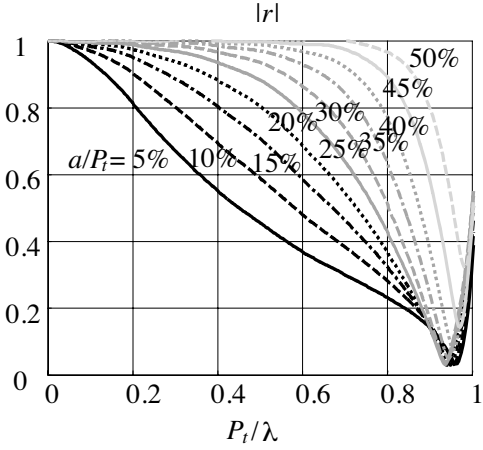

Figure 3. Coefficient $|r|$ versus normalized frequency P_t/λ for different values of a/P_t (FDTD).

reflection coefficient r, φ_r, is also reported in Fig. 4, versus normalized frequency P_t/λ, for different values of the ratio a/P_t. These results will be applied in the next sections in order to characterize structures with multiple layers of PRSs.

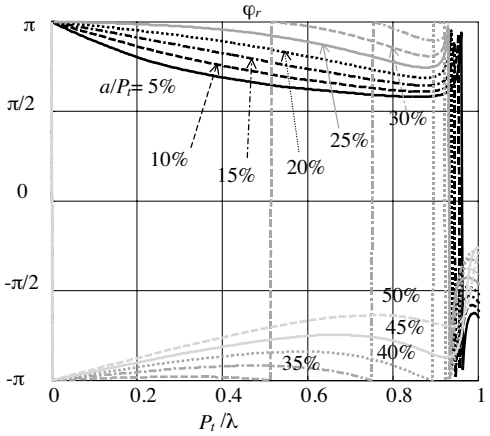

Figure 4. Phase of the reflection coefficient φ_r versus normalized frequency P_t/λ for different values of a/P_t (FDTD).

3. EXCITATION FROM OUTSIDE

In this section, the previous results for the PRS, are used for the characterization of EBG structures composed of multiple layers of PRSs. The EBG structures are illuminated by a plane wave from outside, and they are finite in the direction of wave-propagation. In the following subsections, and in all the paper, the energy conservation relation $|t^2| = 1 - |r|^2$, which is verified because no absorption occurs, will be used to simplify analytical expressions.

3.1. Two Layer Structure

The Fabry-Perot cavity composed of two layers of PRSs separated by the distance D, and illuminated by a plane wave at its left, as illustrated in Fig. 5, is considered. Considering the multiple reflections inside the cavity, and considering only single mode interactions between layers, the amplitude of the total transmitted wave t_2 in the right part and of the total reflected wave in the left part r_2 can be written as following [18]:

$$t_2 = t^2 \sum_{n=0}^{\infty} r^{2n} e^{-jk(2n+1)D} = \frac{t^2 e^{-jkD}}{1 - r^2 e^{-j2kD}} = \frac{t^2 e^{-jkD}}{1 - |r|^2 e^{-j(2kD - \varphi_r)}} \quad (1)$$

$$r_2 = r + \frac{t^2 r e^{-j2kD}}{1 - r^2 e^{-j2kD}} \quad (2)$$

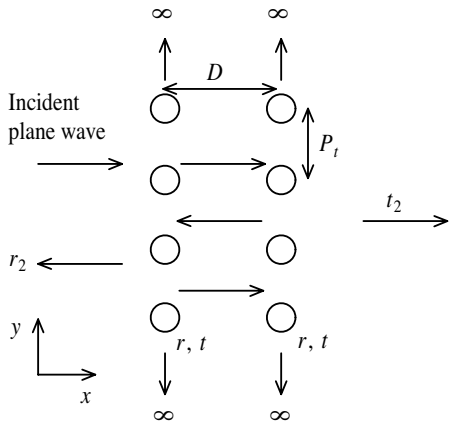

Figure 5. Fabry-Perot cavity excited by a plane-wave source from outside.

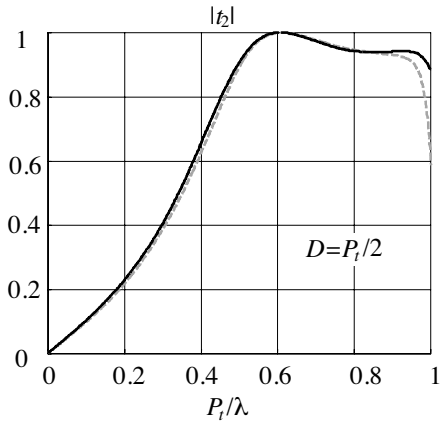

Figure 6. Coefficient $|t_2|$ for $D = P_t/2$, $a/P_t = 5\%$: FDTD (solid line) and semi-analytical model (dashed line).

where k is the free space wave number.

In Figs. 6 to 8, are compared the coefficients $|t_2|$ given by FDTD and those obtained by the hybrid method, for $a/P = 0.5\%$. Different values of the distance D are tested: $D = 0.5P_t$, $D = P_t$ and $D = 2P_t$. From these figures, it can be seen that semi-analytical method gives the same results than the full-wave method (FDTD) for $P_t < 0.8\lambda$. In Figs. 9 to 11, the ratio $a/P = 30\%$ is now considered, and D vary by

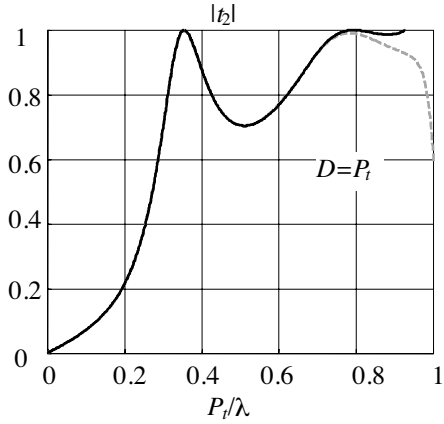

Figure 7. Coefficient $|t_2|$ for $D = P_t$, $a/P_t = 5\%$: FDTD (solid line) and semi-analytical model (dashed line).

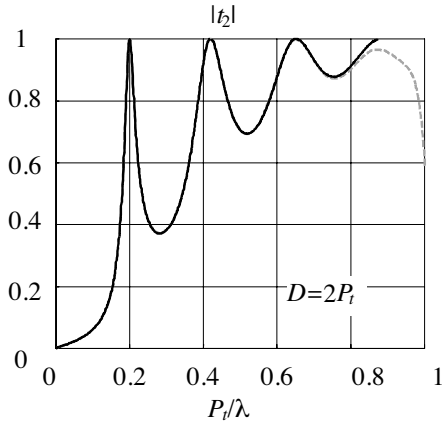

Figure 8. Coefficient $|t_2|$ for $D = 2P_t$, $a/P_t = 5\%$: FDTD (solid line) and semi-analytical model (dashed line).

the same way than previously. One can note that for $D = 0.5P_t$ the hybrid method is less accurate. But for $D \geq P_t$ and $P_t/\lambda < 0.8\lambda$, the two method present the same results.

Eq. (1) is now used in order to study the shape and the resonance frequencies of the transmission coefficient t_2. The resonance picks, are obtained when all the transmitted partial waves have the same phase.

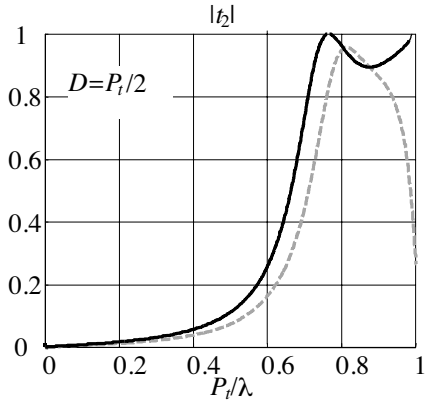

Figure 9. Coefficient $|t_2|$ for $D = P_t/2$, $a/P_t = 30\%$: FDTD (solid line) and semi-analytical model (dashed line).

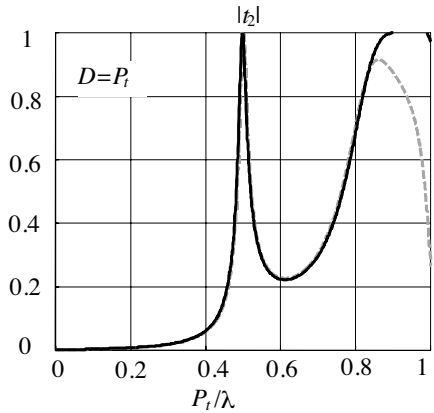

Figure 10. Coefficient $|t_2|$ for $D = P_t$, $a/P_t = 30\%$: FDTD (solid line) and semi-analytical model (dashed line).

This can be written as following:

$$\varphi_r = kD - n\pi, n = 0, \pm 1 \ldots \tag{3}$$

where φ_r is the phase of r. At the resonance frequencies, the maximum value achieved by magnitude of the transmission coefficient t_2 is then given by:

$$|t_2|_{max} = \frac{|t|^2}{1 - |r|^2} = \frac{1 - |r|^2}{1 - |r|^2} = 1 \tag{4}$$

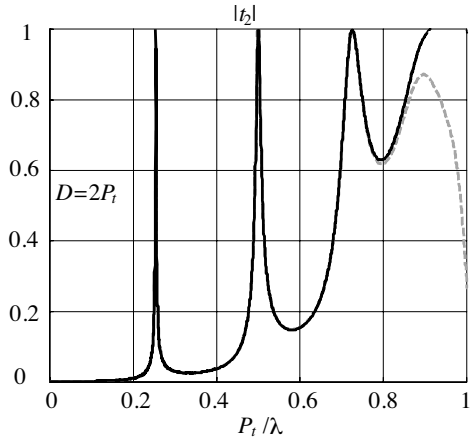

Figure 11. Coefficient $|t_2|$ for $D = 2P_t$, $a/P_t = 30\%$: FDTD (solid line) and semi-analytical model (dashed line).

The envelop of the minima is obtained when the transmitted partial waves have opposite phase. This condition can be written as following:

$$\varphi_r = kD + \pi/2 - n\pi, n = 0, \pm 1 \ldots \tag{5}$$

The envelop of the minima can then be expressed as following:

$$|t_2|_{min} = \frac{|t|^2}{1 + |r|^2} = \frac{1 - |r|^2}{1 + |r|^2} \tag{6}$$

Fig. 12 shows t_2, the phase of r (φ_r) and the lines $kD - n\pi$ ($n = 0, 1 \ldots$), for $D = P_t$ and $a/P_t = 5\%$. The intersections between φ_r and $kD - n\pi$ correspond to the resonance peaks. Fig. 13 illustrate the envelop of the minima and of the maxima for $|t_2|$. Fig. 14 illustrates that the intersections between φ_r and $kD + \pi/2 - n\pi$ correspond to the minima of $|t_2|$. Fig. 15 illustrates the influence of a/P_t in the position of the resonance peaks.

3.2. Multilayered Structures

In this section, the study is extended to multilayered structures. The structure of three layers equally spaced with the longitudinal period P_l, as illustrated in Fig. 16 is considered. By replacing the two first layers by an equivalent surface of characteristics t_2 and r_2, the coefficients of

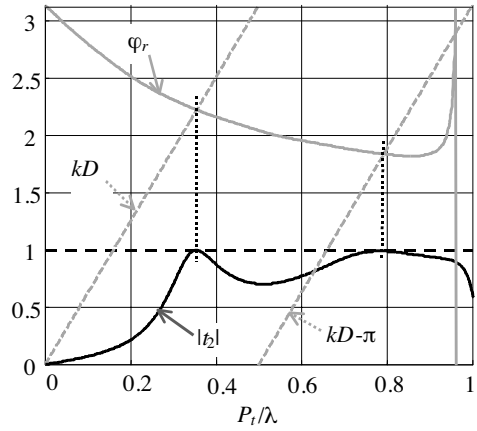

Figure 12. The intersections between φ_r and $kD - n\pi$, $n = 0, 1, \ldots$, correspond to the transmission peaks of $|t_2|$.

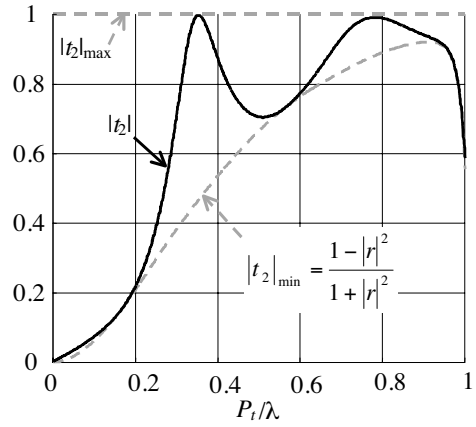

Figure 13. Magnitude $|t_2|$, minima and maxima envelops of this coefficient.

the three layers structure are written as following:

$$t_3 = \frac{t_2 t e^{-jkP_l}}{1 - r_2 r e^{-j2kP_l}} \tag{7}$$

$$r_3 = r_2 + \frac{t_2^2 r e^{-j2kP_l}}{1 - r_2 r e^{-j2kP_l}} \tag{8}$$

Fig. 15 shows results for the coefficient $|t_3|$ obtained with the

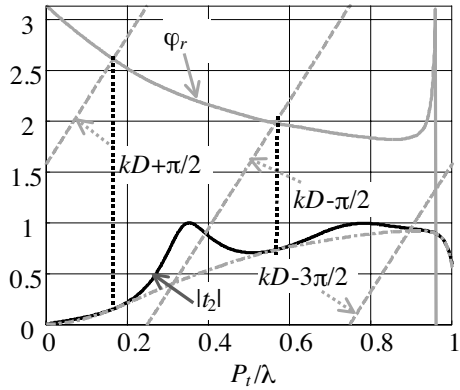

Figure 14. The intersections between φ_r and $kD + \pi/2 - n\pi$, $n = 0, 1, \ldots$, correspond to the minima of $|t_2|$.

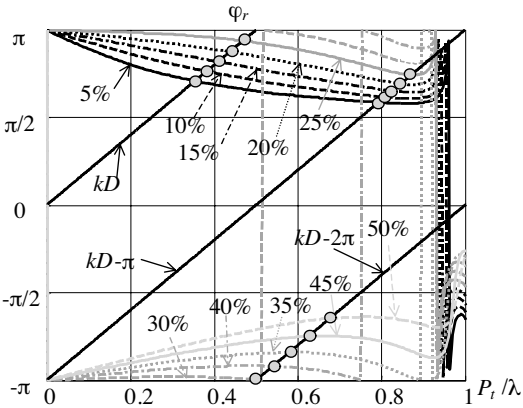

Figure 15. Resonance frequency for different values of a/P_t, with $D = P_t$.

hybrid method those obtained by FDTD. From these curves, Eq. (7) is exact until the normalized frequency $P_t/\lambda < 0.7$.

$|t_3|$ has two peaks in each sides of the peaks of $|t_2|$ (see Fig. 18). By observing that when $|t_2| = 1$, and then $|r_2| = 0$, $|t_3|$ is in a minimum between the resonance peaks, the envelop of this minimum is then given by: $|t_3| = |t|/(1 - 0) = |t|$. Furthermore, the resonance peaks of $|t_3|$ appear for $|t_2| = |t|$. The coefficients $|t|$, $|t_2|$ and $|t_3|$ are plotted in Fig. 18, to illustrate that the intersections between $|t_2|$ and $|t|$ correspond to the resonance peaks of $|t_3|$ and that between two

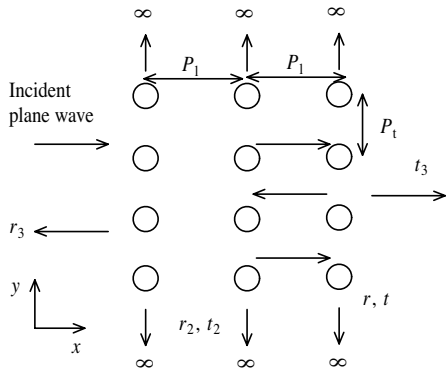

Figure 16. Three layers of partially reflecting surfaces excited by a plane-wave source from outside.

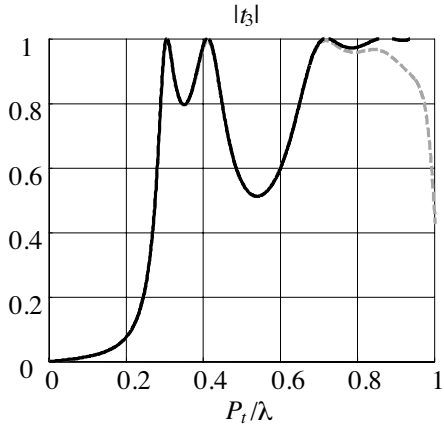

Figure 17. Magnitude of the transmission coefficient $|t_3|$ for the three-layers structure, for $P_l = P_t$, $a/P_t = 5\%$: FDTD (solid line) and semi-analytical model (dashed line).

peaks of $|t_3|$ the minimum is given by $|t|$.

By generalizing to n layers, it is obtained the following iterative equations, for the transmission and reflection coefficients:

$$t_n = \frac{t_{n-1} t e^{-jkP_l}}{1 - r_{n-1} r e^{-j2kP_l}} \tag{9}$$

$$r_n = r_{n-1} + \frac{t_{n-1}^2 r e^{-j2kP_l}}{1 - r_{n-1} r e^{-j2kP_l}} \tag{10}$$

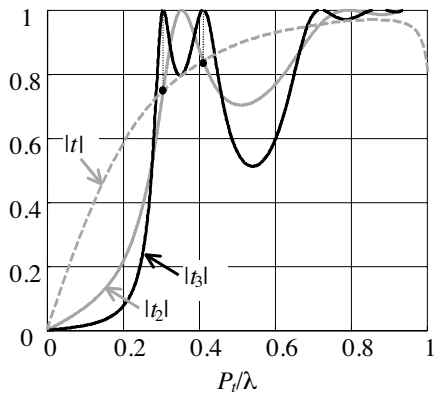

Figure 18. Coefficients $|t|$, $|t_2|$, and $|t_3|$. The intersections between $|t|$ and $|t_2|$ correspond to the peaks of $|t_3|$. The minimum between two peaks of $|t_3|$ is determined by $|t|$.

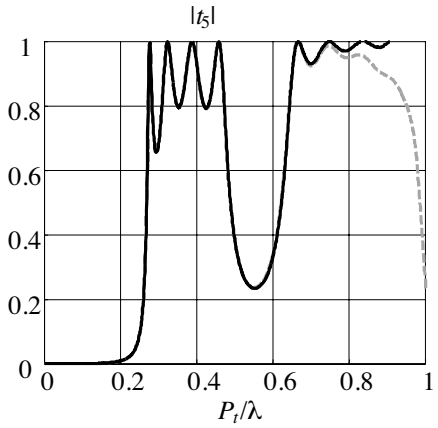

Figure 19. Coefficient $|t_5|$ for $P_l = P_t$, $a/P_t = 5\%$: FDTD (solid line) and semi-analytical model (dashed line).

In Fig. 19, the magnitude of $|t_n|$ is plotted, for $n = 5$, using both, FDTD and semi-analytical methods, showing the accuracy of the hybrid method for $P_t/\lambda < 0.7$. It is interesting to note that the transmission peaks of $|t_n|$ appear at the intersections between $|t_{n-1}|$ and $|t|$. Indeed, this conducts to $|t_n| = |t_{n-1}||t|/(1 - |r_{n-1}||r|) = |t_{n-1}|^2/(1 - |r_{n-1}|^2) = 1$, at these resonance frequencies.

From Eq. (9), the envelop of the minima for $|t_n|$ can be written as

following:

$$|t_n|_{min} = \frac{|t_{n-1}t|}{1+|r_{n-1}r|} \tag{11}$$

To obtain a simpler expression, the corresponding maxima of $|r_n|$ are first calculated. By using $|r_n|^2_{max} = 1 - |t_n|^2_{min}$, $|t_{n-1}|^2 = 1 - |r_{n-1}|^2$ and $|t|^2 = 1 - |r|^2$, the following relation is obtained:

$$|r_n|_{max} = \frac{|r| + |r_{n-1}|}{1+|r_{n-1}r|} \tag{12}$$

In order to simplify this equation, we consider the coefficient $f_n = \frac{1-|r_n|_{max}}{1+|r_n|_{max}}$. After some algebra, it is obtained $f_n = \frac{1-|r|}{1+|r|}\frac{1-|r_{n-1}|}{1+|r_{n-1}|}$, and then $f_n = \left(\frac{1-|r|}{1+|r|}\right)^n$. From this, the envelop of the maxima for $|r_n|$ is given by

$$|r_n|_{max} = \frac{1-\left(\frac{1-|r|}{1+|r|}\right)^n}{1+\left(\frac{1-|r|}{1+|r|}\right)^n} \tag{13}$$

The corresponding envelop of the minima for $|t_n|$ is then written as following:

$$|t_n|_{min} = \frac{2\left(\frac{1-|r|}{1+|r|}\right)^{n/2}}{1+\left(\frac{1-|r|}{1+|r|}\right)^n} \tag{14}$$

The coefficients $|t_2|$, $|t_3|$, $|t_4|$, and $|t_5|$ and their minima envelops are reported in Fig. 20. The coefficients $|r_2|$, and $|r_5|$ and their maxima envelops are plotted in Fig. 21.

4. EXCITATION FROM INSIDE

In this section, the plane-wave source is considered inside the Fabry-Perot cavity or the EBG structure. For this case, the same ray analysis than previously is carried out.

4.1. Analysis of the "Transmission" Coefficient

4.1.1. Two Layers Structure

Two layers of PRSs are considered at the same distance $D/2$ at each side of the source as illustrated in Fig. 22(a). The source is considered transparent to electromagnetic waves and it sends two plane waves on each side. In the FDTD code, the source is modeled with a plane of current sources. Another model of the source, which considers

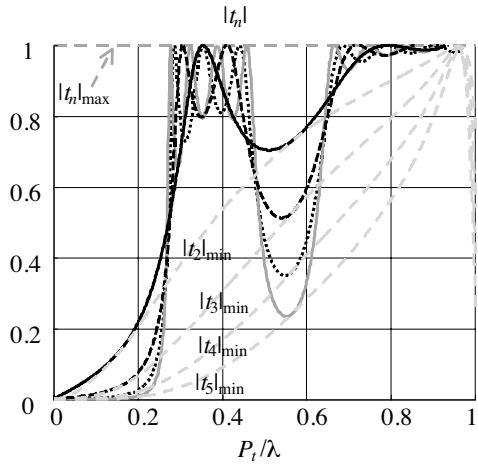

Figure 20. Coefficients $|t_2|$, $|t_3|$, $|t_4|$, and $|t_5|$ and their minima envelops.

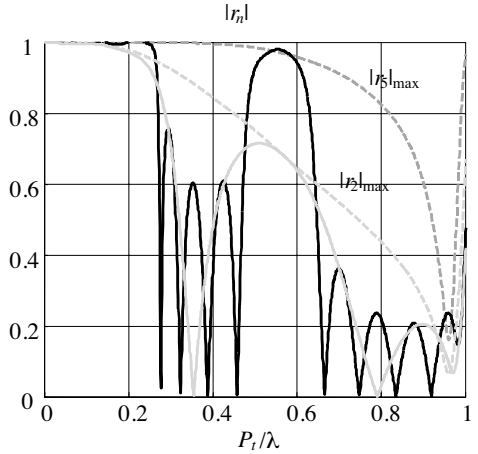

Figure 21. Coefficients $|r_2|$ and $|r_5|$ and their maxima envelops.

the interactions of the source with the electromagnetic waves inside the cavity will be presented later in this paper. Because of the reciprocity principle, this analysis is equivalent to the one of the problem illustrated in Fig. 22(b), where the Fabry-perot cavity is excited from outside and the total wave is calculated at the center of the cavity. As referring to Fig. 22(a), the amplitude of the total transmitted wave T_2 is calculated by summing the rays outside the

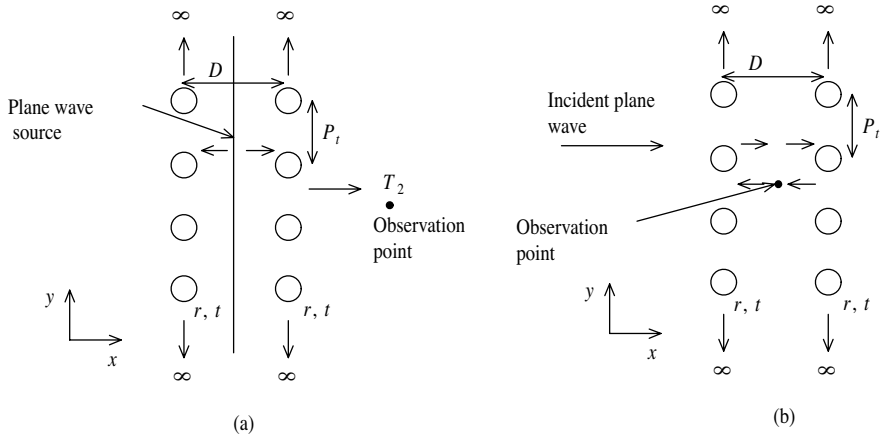

Figure 22. Two equivalent problems: (a) Fabry-Perot cavity excited by a plane wave source from its inside. Calculation of the total transmitted wave outside the cavity (b) Fabry-Perot cavity excited by a plane wave source from outside. Calculation of the wave inside the cavity.

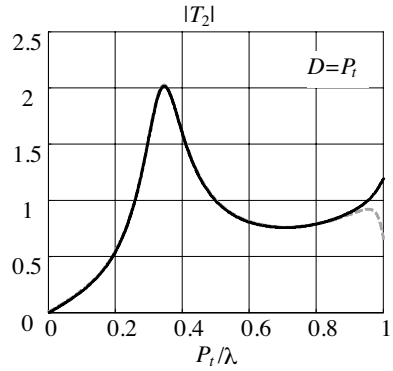

Figure 23. Coefficient $|T_2|$ for $D = P_t$, $a/P_t = 5\%$: FDTD (solid line) and semi-analytical model (dashed line).

cavity:

$$T_2 = t \sum_{n=0}^{\infty} r^n e^{-jk(2n+1)D/2} = \frac{te^{-jkD/2}}{1 - re^{-jkD}} \tag{15}$$

$|T_2|$ is plotted in Fig. 23, for $a/P_t = 5\%$ and $D = P_t$, by using FDTD

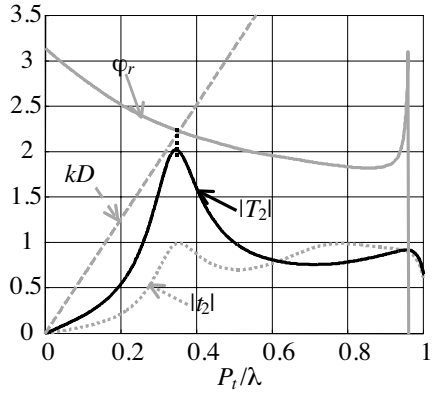

Figure 24. Intersections between φ_r and $kD - 2n\pi$, $n = 0, 1, \ldots$, correspond to transmission peaks of $|T_2|$. $|t_2|$ has one more peaks than $|T_2|$.

and semi-analytical method. For T_2, the resonance condition is written:

$$\varphi_r = kD - 2n\pi, \quad n = 0, \pm 1 \ldots \tag{16}$$

This condition is illustrated in Fig. 24 for $D = P_t$. In this figure, the coefficient $|t_2|$ is also plotted, in order to show that $|t_2|$ has twice more resonance frequencies than $|T_2|$. The minima envelop is written as following:

$$\varphi_r = kD - (2n+1)\pi, \quad n = 0, \pm 1 \ldots \tag{17}$$

The envelop of maxima for $|T_2|$ is given by:

$$|T_2|_{max} = \frac{|t|}{1-|r|} = \frac{\sqrt{1-|r|^2}}{1-|r|} = \sqrt{\frac{1+|r|}{1-|r|}} \tag{18}$$

From Eq. (18), $|T_2|_{max}$ is equal or greater than one and can theoretically become very large if $|r|$ is near one (note that $0 \leq |r| < 1$). This means that the source inside the cavity can supply more power in the presence of the cavity than without the cavity. This is due to the fact that the cavity modifies the matching of the source to free space. Taking into account the available power from the source, a normalized version for the transmission coefficient will be proposed later in this paper.

The envelop of minima for $|T_2|$ is expressed as following:

$$|T_2|_{min} = \frac{|t|}{1+|r|} = \frac{\sqrt{1-|r|^2}}{1+|r|} = \sqrt{\frac{1-|r|}{1+|r|}} = \frac{1}{|T_2|_{max}} \tag{19}$$

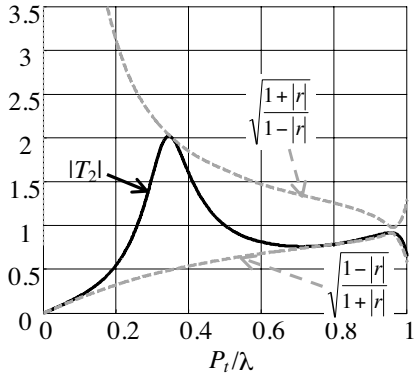

Figure 25. Coefficient $|T_2|$, envelops of minima and maxima.

The coefficient $|T_2|$, the envelops of minima and maxima are plotted in Fig. 25, for $D = P_t$, and in Fig. 29, for $D = 2P_t$.

4.1.2. Multilayered Structure

Multiple PRSs are on each sides of the source. The case $P_l = D = 2P_t$ is considered. For n layers periodically spaced by the distance P_l, at the distance $P_l/2$ at each sides of the source, one can show that the coefficient T_{2n} is written:

$$T_{2n} = \frac{t_n e^{-jkP_l/2}}{1 - r_n e^{-jkP_l}} \tag{20}$$

In Eq. (20), t_n and r_n are obtained from Eqs. (9) and (10).

The coefficient $|T_{2n}|$ for $n = 4$ is plotted in Fig. 26. In this figure, this coefficient is compared to the transmission coefficients of the cavity walls (*i.e.*, $|t_n|$) and in Fig. 27, it is compared to the transmission coefficient of the all structure excited from outside (*i.e.*, $|t_{2n}|$). From these curves, the coefficient $|T_{2n}|$ has one more peak than $|t_n|$ in the first pass-band, but the two coefficients have the same number of peaks in the second pass-band (Fig. 26). In addition, the first peak of $|T_{2n}|$ occurs at the same frequency that the first peak of $|t_{2n}|$ (Fig. 27).

4.2. Concerning the Strength of "Transmission" Coefficient Greater than One

The strength of the coefficient greater than one is due to the fact that the power supplied by the source has not been considered. In the

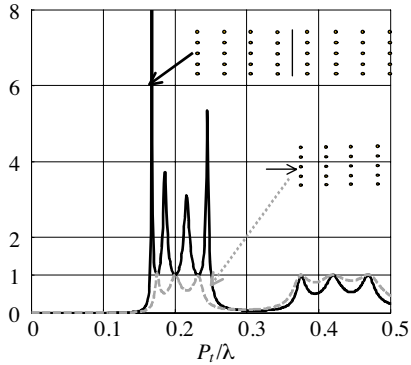

Figure 26. Coefficient $|T_{2n}|$, for $n = 4$ and coefficient $|t_4|$. $P_l = D = 2P_t$ and $a/P_t = 5\%$. In the first pass-band, $|T_{2*4}|$ has two more peaks than $|t_4|$. In the second pass-band the two coefficients have the same number of peaks.

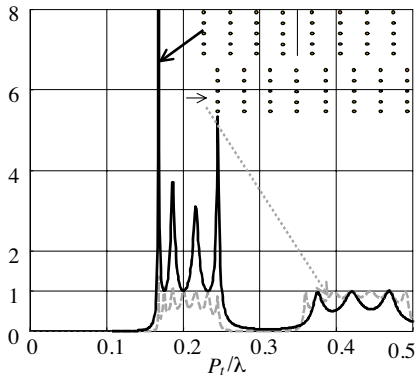

Figure 27. Coefficient $|T_{2n}|$, for $n = 4$ and coefficient $|t_8|$. $P_l = D = 2P_t$ and $a/P_t = 5\%$. The first peak of $|T_{2n}|$ occurs at the same frequency that the first peak of $|t_{2n}|$.

next sub-sections, a normalized version for this coefficient, which take into account the power available by the source is proposed, by using a transmission line model.

4.2.1. Power Normalization

The Fabry-Perot cavity excited from its inside (see Fig. 22(a)) is represented by the transmission line model as illustrated in Fig. 28(a).

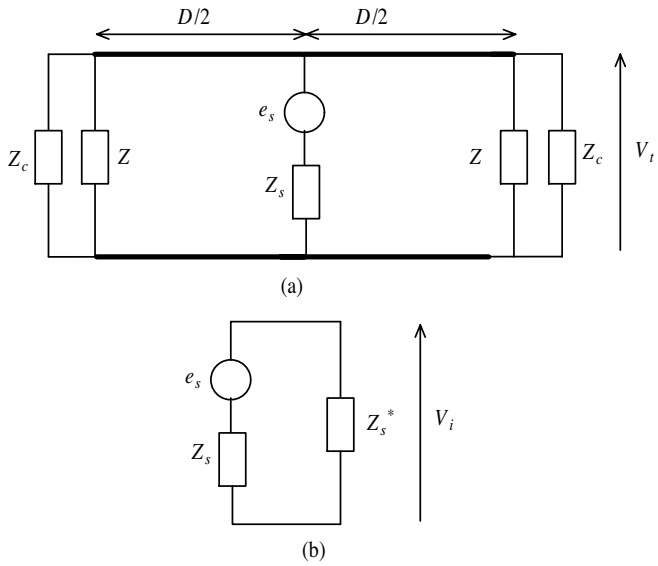

Figure 28. Transmission line models: (a) Source-fabry perot cavity structure (b) Source with matched impedance.

In Fig. 28(b), the transmission line model of the source with its matched impedance is also presented in order to calculate the available power from the source. Z_c is the free-space characteristic impedance ($Z_c = 120\pi$). Z is the equivalent circuit model of the PRS. Z_s and e_s are the equivalent impedance and equivalent tension of the source, respectively.

To calculate the transmission coefficient outside the cavity, the available power P_i (see Fig. 28(b)) is first calculated [19]:

$$P_i = \frac{1}{2}\frac{|V_i|^2}{Z_s^*} = \frac{1}{2}\frac{|Z_s^*|^2}{Z_s^*|Z_s^* + Z_s|^2}|e_s|^2 \tag{21}$$

where e_s, Z_s and V_i parameters are shown in Fig. 28(b). Then, referring to Fig. 28(a), the transmitted power P_t for one side of the transmission line is given by:

$$P_t = \frac{1}{2}\frac{|V_t|^2}{Z_c} \tag{22}$$

The transmission and reflection coefficients t and r can be expressed as functions of Z as following [19]:

$$t = \frac{2Z}{2Z + Z_c} \tag{23}$$

$$r = -\frac{Z_c}{2Z + Z_c} \tag{24}$$

t_s and r_s are the transmission and reflection coefficients of the source and can be written as functions of Z_s

$$t_s = \frac{2Z_s}{2Z_s + Z_c} \tag{25}$$

$$r_s = -\frac{Z_c}{2Z_s + Z_c} \tag{26}$$

By using Eqs. (23)–(26), and after simplification (see Appendix), one can show that Eq. (22) can be written

$$P_t = \frac{1}{2}\frac{Z_c}{|2Z_s + Z_c|^2}\frac{|te^{-jkD/2}|^2}{|1 - r(r_s + t_s)e^{-jkD}|^2}|e_s|^2 \tag{27}$$

Taking into account the power transmitted from the both sides of the line, the normalized squared magnitude of the transmission coefficient $|T_2|^2_{Norm,max}$ can be expressed as following:

$$|T_2|^2_{Norm,max} = \frac{2P_t}{P_i} = \frac{2Z_c Z_s^*|Z_s^* + Z_s|^2}{|Z_s^*|^2|2Z_s + Z_c|^2}\frac{|te^{-jkD/2}|^2}{|1 - r(r_s + t_s)e^{-jkD}|^2} \tag{28}$$

For the case of real Z_s, Eq. (12) becomes

$$|T_2|^2_{Norm,max} = 4|r_s||t_s|\frac{|te^{-jkD/2}|^2}{|1 - r(r_s + t_s)e^{-jkD}|^2} \tag{29}$$

The maximum is then written

$$|T_2|^2_{Norm,max} = 4|r_s||t_s|\frac{1 - |r|^2}{(1 - |r||r_s + t_s|)^2} \tag{30}$$

In Fig. 29, $|T_2|^2_{Norm,max}$ is plotted versus Z_s for different values of $|r|$. From these curves, one can see that the strength of $|T_2|^2_{Norm,max}$ is always limited to 1, as expected.

4.2.2. Discussion

To analyze the directivity of an antenna embedded inside a Fabry-Perot cavity, one can use Eq. (15), where the variable D is replaced by $D\cos(\theta)$, and θ is the angle of the transmitted waves. This analysis has been recently presented in [20]. The directivity has been predicted

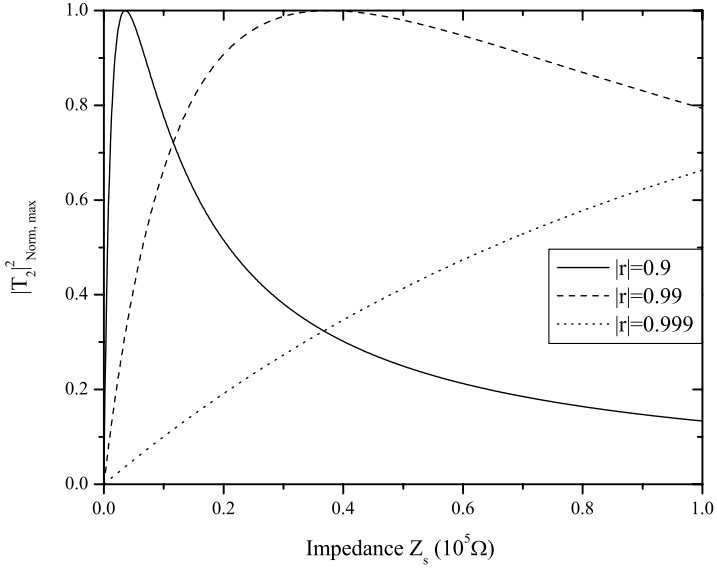

Figure 29. $|T_2|^2_{Norm,max}$ coefficient versus Z_s for different values of $|r|$.

by considering the angular dependance of the transmission coefficient. The Fabry-Perot cavity increases the directivity of the antenna and then its gain. Indeed, the relationship between directivity and gain for highly directive antennas is well known [21]. However, it can be noted that the strength of the coefficient of Eq. (15), can not be interpreted has the gain of this antenna, because it does not consider the power available by the source.

Theoretically the coefficient of Eq. (29), is more correct than the coefficient of Eq. (15). However, it is less applicable in practice, because we don't have necessarily access to the transmission and reflection coefficients of the source.

A rapid comparison between Eq. (15) and Eq. (29) shows that the normalized version (Eq. (29)) has two factors more: $4|r_s||t_s|$ and $(r_s + t_s)$ (in the denominator). For directive-antennas incorporating a Fabry-Perot cavity, we focus on the angular dependence of the transmission coefficient. If the source is omnidirectional, the factor $4|r_s||t_s|$ is independent on transmitting angle and can then be omitted. Furthermore, as the source can usually considered as a point source, it can be considered having negligible interaction with the reflecting plane-waves inside the cavity, which leads to $r_s \approx 0$, $t_s \approx 1$ and $r_s + t_s \approx 1$. From these, using the coefficient version presented in

Eq. (15) for predicting the radiation patterns of directive-antennas based on a Fabry-Perot cavity excited internally is justified. However, the strength of this coefficient should not be considered as the gain of these antennas. The observed improvement of the gain of these antennas is more associated with the enhancement of their directivity that can be evaluated by calculating the half power beamwidth by using Eq. (15) (with D replaced by $D\cos(\theta)$) as has been demonstrated in [20].

5. CONCLUSION

A new analysis of Electromagnetic Band Gap structures (EBGs) composed of multiple Partially Reflecting Surfaces (PRSs) of metallic wires has been presented. Transmission coefficients, for a plane-wave excitation, obtained with a semi-analytical method, which considers only the fundamental mode interaction between PRSs, have been validated by comparing them with the results of a full-wave method (FDTD). The shape and the resonance frequencies of the transmission coefficients have been studied by using analytical expressions. The two cases, excitation from outside and excitation from inside, have been treated. For the inside-excitation case, the transmission coefficient presents a different number of resonance peaks than for the outside-excitation case. A discussion is also presented concerning the strength of the coefficient greater than one obtained when the plane-wave source is inside the EBG structure. In addition, by using a transmission line model, a normalized version for this coefficient is proposed, which considers the available power by the source. This work is useful for the design process of multilayered periodic structures and for physical study of crystals excited internally, which has applications in the design of high-gain antennas.

APPENDIX A.

The details for the calculation of the variable V_t (see Fig. 28(a)) are given in this appendix. Fig. A1 presents the equivalent model for the circuit of Fig. 28(a).

In this Figure, the impedance Z' can be written as following:

$$Z' = \frac{Z_c}{2}\frac{Z//Z_c + j\tan kD/2}{Z//Z_c + j\tan kD/2} = \frac{Z_c}{2}\frac{1-\frac{Z_c}{2Z+Z_c}e^{-jkD}}{1+\frac{Z_c}{2Z+Z_c}e^{-jkD}} = \frac{Z_c}{2}\frac{1-re^{-jkD}}{1+re^{-jkD}} \tag{A1}$$

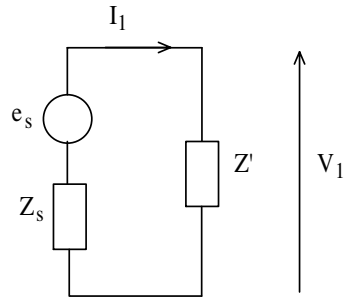

Figure A1. Equivalent transmission line model of Fig. 28(a).

The expression for the voltage V_1 (see Fig. A1) can be written:

$$V_1 = \frac{Z'}{Z' + Z_s} e_s = \frac{Z_c(1 + re^{-jkD})}{(2Z_s + Z_c) - (2Z_s - Z_c)re^{-jkD}} e_s \tag{A2}$$

And the current I_1 is expressed as following:

$$I_1 = \frac{V_1}{Z'} = 2\frac{1 - re^{-jkD}}{(2Z_s + Z_c) - (2Z_s - Z_c)re^{-jkD}} e_s \tag{A3}$$

Then the voltage V_t (Fig. 28(a)) is deduced from these results:

$$\begin{aligned} V_t &= V_1 \cos(kD/2) + jZ_c I_1/2 \sin(kD/2) \\ &= \frac{Z_c(1 + r)e^{-jkD/2}}{(2Z_s + Z_c) - (2Z_s - Z_c)re^{-jkD}} \\ &= \frac{Z_c}{2Z_s + Z_c} \frac{(1 + r)e^{-jkD/2}}{1 - \dfrac{2Z_s - Z_c}{2Z_s + Z_c} re^{-jkD}} \\ &= \frac{Z_c}{2Z_s + Z_c} \frac{te^{-jkD/2}}{1 - (r_s + t_s)re^{-jkD}} \end{aligned} \tag{A4}$$

REFERENCES

1. Yablonovitch, E., "Inhibited spontaneous emission in solid state physics," *Physical Review Letters,* Vol. 58, No. 20, 2059–2062, 1987.
2. Joannopoulos, J., R. D. Meade, and J. N. Winn, *Photonic Crystals: Molding the Flow of Light,* Princeton University Press, 1995.

3. Yang, F. and Y. Rahmat-Samii, "Microstrip antennas integrated with electromagnetic bandgap (EBG) structures: a low mutual coupling design for array applications," *IEEE Trans. on Antennas Prop.*, Vol. 51, 2936–2946, Oct. 2003.
4. Poilasne, G., P. Pouliguen, K. Mahdjoubi, L. Desclos, and C. Terret, "Active metallic photonic band-gap materials (MPBG): experimental results on beam shaper," *IEEE Trans. on Antennas Prop.*, Vol. 48, 117–119, Jan. 2000.
5. Lourtioz, J. M., A. De Lustrac, F. Gadot, S. Rowson, A. Chelnokov, T. Brillat, A. Ammouche, J. Danglot, O. Vanbesien, and D. Lippens, "Toward controllable photonic crystals for centimeter and millimeter wave devices," *Journal of Lightwave Technology*, Vol. 17, 2025–2031, Nov. 1999.
6. Thevenot, M., C. Cheype, A. Reineix, and B. Jecko, "Directive photonic band-gap antennas," *IEEE Trans. Microwave Theory Tech.*, Vol. 47, 2115–2122, Nov. 1999.
7. Cheype, C., C. Serier, M. Thevenot, T. Monediere, A. Reineix, and B. Jecko, "An electromagnetic bandgap resonator antenna," *IEEE Trans. on Antennas Prop.*, Vol. 50, 1285–1290, Sept. 2002.
8. Biswas, R., E. Ozbay, B. Temelkuran, M. Bayandir, M. Sigalas, and K.-M. Ho, "Exceptionally directional sources with photonic band-gap crystals," *Optical Society of America*, Vol. 18, No. 11, 1684–1689, Nov. 2001.
9. Akalin, A., J. Danglot, O. Vanbesien, and D. Lippens, "A highly directive dipole antenna embedded in a fabry-perot type cavity," *IEEE Microwave Wireless Comp. Lett.*, Vol. 12, 48–50, Feb. 2002.
10. Enoch, S., G. Tayeb, P. Sabouroux, N. Guerin, and P. Vincent, "A metamaterial for directive emission," *Phys. Rev. Lett.*, Vol. 89, No. 21, 213902-1-213902-4, Nov. 2002.
11. Felbacq, D., G. Tayeb, and D. Maystre, "Scattering by a random set of parallel cylinders," *J. Opt. Soc. Am. A*, Vol. 11, 2526–2538, Sept. 1994.
12. Hall, R. C., R. Mittra, and K. M. Mitzner, "Analysis of multilayered periodic structures using generalized scattering matrix," *IEEE Trans. on Antennas Prop.*, Vol. 36, 111–117, Apr. 1988.
13. Munk, B. A., *Frequency Selective Surfaces: Theory and Design,* Wiley-Interscience Publication, 2000.
14. De Lima, A. C. and E. A. Parker, "Fabry-Perot approach to the design of double layer FSS," *IEE Proc. Microwave Antennas Propagat.*, Vol. 143, 157–162, Apr. 1996.

15. Lee, S. W., G. Zarrillo, and C. L. Law, "Simple formulas for transmission through grids or plates," *IEEE Trans. on Antennas Prop.*, Vol. 30, 904–909, Sept. 1982.
16. Ozbay, E., B. Temelkuran, and M. Bayindir, "Microwave applications of photonic crystals," *Progress In Electromagnetics Research*, PIER 41, 185–209, 2003.
17. Guida, G., P. N. Stavrinou, G. Parry, and J. B. Pendry, "Time reversal symmetry, microcavities and photonic crystals," *Journ. Modern. Opt.*, Vol. 48, 581–595, 2001.
18. Hecht, E., *Optics*, 421–425, Addison Wesley, San Francisco, CA, 1988.
19. Pozar, D., *Microwave Engineering*, 2nd ed., Wiley, New York, 1998.
20. Boutayeb, H., K. Mahdjoubi, A. C. Tarot, and T. Denidni, "Directivity of an antenna embedded inside a Fabry-Perot cavity: Analysis and design," *Microw. Opt. Technol. Lett.*, Vol. 48, 12–17, Jan. 2006.
21. Balanis, C. A., *Antenna Theory: Analysis and Design*, second edition, 46, 600, John Wiley and Sons, 1997.